International Journal of Thermophysics, Vol. 26, No. 3, May 2005 (© 2005)
DOI: 10.1007/s10765-005-5585-3

Thermophysical Property Measurements of Liquid and Supercooled Iridium by Containerless Methods

T. Ishikawa,[1,2] P.-F. Paradis,[1] R. Fujii,[3] Y. Saita,[4] and S. Yoda[1]

Received August 9, 2004

Thermophysical properties of equilibrium and supercooled liquid iridium were measured using noncontact diagnostic techniques in an electrostatic levitator. Over the 2300–3000 K temperature range, the density can be expressed as $\rho(T) = 19.5 \times 10^3 - 0.85(T - T_m)$ (kg·m^{-3}) with $T_m = 2719$ K. The volume expansion coefficient is given by 4.4×10^{-5} K^{-1}. In addition, the surface tension can be expressed as $\gamma(T) = 2.23 \times 10^3 - 0.17(T - T_m)(10^{-3}$N·m$^{-1})$ over the 2373–2833 K span and the viscosity as $\eta(T) = 1.85 \exp[3.0 \times 10^4/(RT)](10^{-3}$Pa·s) over the same temperature range.

KEY WORDS: density; iridium; liquid; surface tension; viscosity.

1. INTRODUCTION

Iridium is known to be the most corrosion-resistant metal, and due to its refractory nature, it has been used for crucibles and apparatus for high temperature applications. Also, it has been used to harden platinum and osmium alloys to make electrical contacts, tipping pens, and compass bearings [1]. In particular, it was used to make the standard meter bar of Paris (90% platinum- 10% iridium alloy). Research on new iridium-based superalloys has recently been conducted to allow operation of gas turbines (jet engine, power plant generator) at higher temperatures [2]. However, because of its high melting point (2719 K) [1] and its reactivity at high temperatures, it is challenging to perform the measurement of thermophysical properties in its liquid state using conventional methods.

[1] Japan Aerospace Exploration Agency, 2-1-1 Sengen, Tsukuba, Ibaraki 305-8505, Japan.
[2] To whom correspondence should be addressed. E-mail: ishikawa.takehiko@jaxa.jp
[3] Chiba Institute of Technology, 2-17-1 Tsudanuma, Narashino, Chiba, Japan.
[4] Advanced Engineering Service Co. Ltd., 1-6-1 Takezono, Tsukuba, Ibaraki, Japan.

A knowledge of its thermophysical properties and their temperature dependence in the liquid state is important for studies on phase transformations, nucleation, atomic dynamics, and surface physics, as well as for industrial processes (e.g., refining, casting, and welding). These properties are also useful when designing alloys because the properties of component elements in the liquid state are required to estimate those of the final alloy (e.g., binary, ternary systems).

In this study, electrostatic levitation in vacuum is used to overcome the contamination problems associated with the conventional high temperature processing and to allow accurate determination of the density, surface tension, and viscosity [3, 4]. This paper first briefly describes the experimental facility and the measurement methods, and then presents the experimental results.

2. EXPERIMENTAL SETUP AND PROCEDURES

2.1. Electrostatic Levitation Furnace

The measurements were made using an electrostatic levitator (Fig. 1) [3, 4] that consisted of a chamber evacuated to a $\sim 10^{-5}$ Pa vacuum level before processing was initiated. The chamber housed a sample charged by electronic emission and levitated between electrodes via a feedback loop (the two disk electrodes are for the vertical position control and the four spherical electrodes are for the horizontal control) [5]. The positioning control relied on two sets of orthogonally arranged He–Ne lasers and the associated position detectors. The three-dimensional sample position information was fed to a computer that produces position (x, y, and z) control voltages to high voltage amplifiers so that a prefixed sample position can be maintained. The lower electrode was surrounded by four coils that generated a rotating magnetic field that was used for rotation control [6]. Specimens were prepared by arc melting 99.9 mass% purity iridium powder (Nilaco Corp., Japan) into spheroids with diameters of ca. 2 mm.

Three laser beams were used for sample heating (Fig. 1). The beam of one CO_2 laser (10.6 μm emission) was sent directly to the sample whereas that from another CO_2 laser was divided into two beams such that the three focused beams in a same plane, separated by 120 degrees, hit the specimen. This configuration provided temperature homogeneity, sample position stability, and helped to control sample rotation.

The radiance temperature was measured with a single-color pyrometer (0.90 μm, 120 Hz acquisition rate) covering a 1200–3800 K interval. Calibration to true temperature was obtained with the help of Planck's law and performed using custom-made Code Warrior^{TM} software. A typical

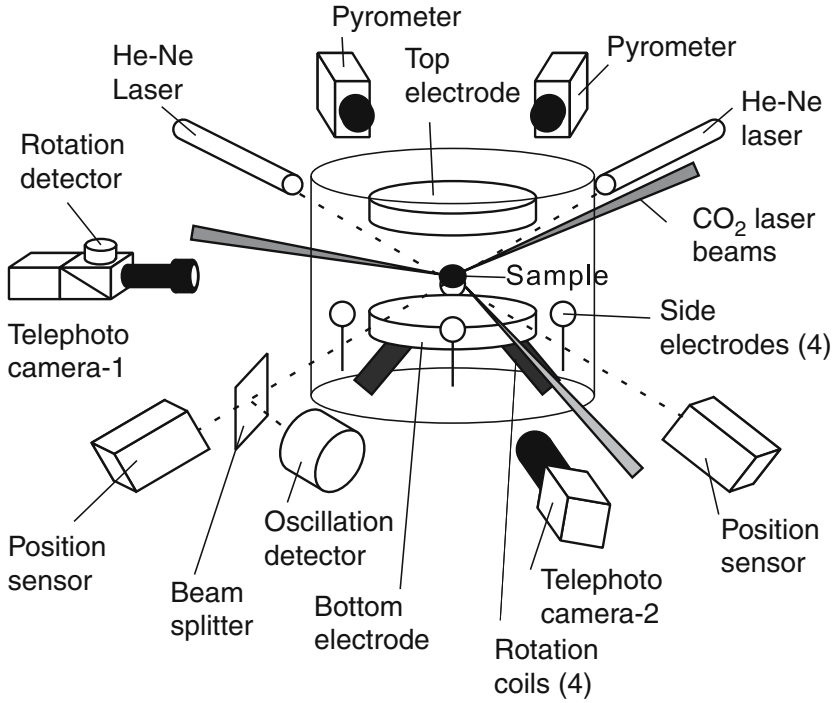

Fig. 1. Schematic view of the electrostatic levitation furnace.

temperature profile for a cooling iridium sample exhibiting 420 K supercooling and recalescence (sudden temperature rise due to the release of the latent heat of fusion of an undercooled sample upon solidification) is shown in Fig. 2.

The sample was observed by three charge-coupled-device (CCD) cameras. One color camera offered a view of both the electrodes and the sample. In addition, two black and white high-resolution cameras (camera-1 and camera-2), located at right angles from each other and equipped with telephoto objectives, provided magnified views of the sample for density measurements. This also helped to monitor the sample position in the horizontal plane and to align the heating laser beams to minimize photon-induced horizontal sample movement and sample rotation [7].

2.2. Thermophysical Properties Determination

Density measurements were carried out using a UV imaging technique described in detail elsewhere [8, 9]. First, a solid sample was

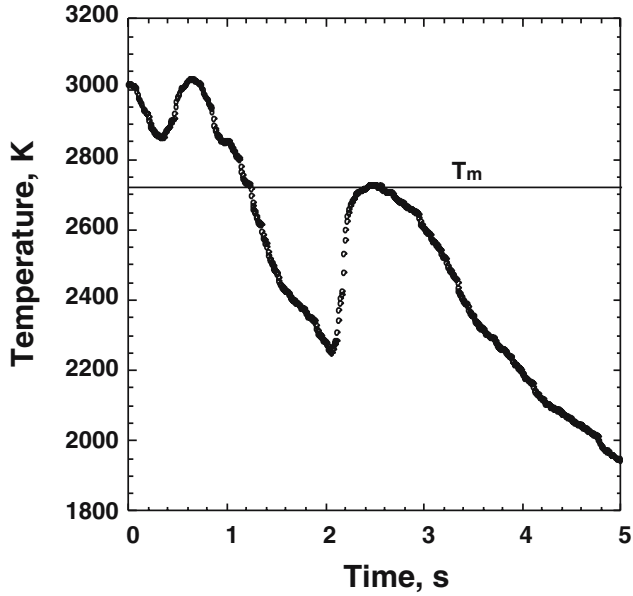

Fig. 2. Radiative temperature profile for a iridium sample showing supercooling and recalescence.

levitated and vertical-axis rotation was induced by a rotating magnetic field. The rotation rate of the solid sample can be measured by a rotation detector, which monitors the intensity of He–Ne lasers reflected from the uneven sample surface [6]. When the rotation rate reached 10 Hz, the rotating magnetic field was turned off. All CO_2 laser beams were directed in such a way to minimize photon-induced rotation during the sample heating. Once a levitated sample was melted (ca. 2 mm diameter, nearly 50 mg), it became spherical due to surface tension and the distribution of surface charge. If the shape of a molten sample departed from that of a sphere (due to excessive rotation), a counter torque was applied by the magnetic field [6] to restore the spherical shape. Moreover, the controlled sample rotation not only improved the temperature homogeneity of the sample [10] but also prevented precession and ensured the axi-symmetry of the sample along the vertical axis.

Images at the rate of 30 frames/s and temperature data were simultaneously recorded as a function of time. All laser beams were then blocked with mechanical shutters allowing the sample to cool radiatively. After the experiment, the video images from one high-resolution camera were digitized. Since the sample was axi-symmetric, the sample volume could

be calculated from each image. The recorded images were calibrated by levitating a brass sphere with a precisely known radius under identical experimental conditions. The images were then matched with the thermal history of the sample (Fig. 2). Because its mass was known, the density could be determined as a function of temperature. Although the sample evaporated as evidenced by a change in radius during long levitation periods (hours), the density experiments lasted a few minutes, for which the melting temperature was exceeded for only a few seconds (Fig. 2). Therefore, the effect on density was negligible.

The surface tension and viscosity were determined by studying the behavior of the sample oscillation about its equilibrium shape [11]. In this method, a solid sample was first levitated, rotated around 10 Hz, heated, melted, and brought to a selected temperature. Then, a $P_2\cos(\theta)$-mode drop oscillation was induced to the sample by superimposing a small sinusoidal electric field on the levitation field. The transient signal that followed the termination of the excitation field was detected and analyzed using a custom-made program. This was done several times at a given temperature and repeated for several temperatures. Using the characteristic oscillation frequency ω_c of the signal, which was calculated by a fast Fourier transform (FFT) analysis and then corrected for nonuniform surface charge distribution, the surface tension γ can be determined from [12]

$$\omega_c^2 = \left(\frac{8\gamma}{\rho r_0^3}\right) Y \tag{1}$$

where r_0 is the radius of the sample, ρ is the density, and Y is the correction factor that depends on the drop charge, the permittivity of vacuum, and the applied electric field [13, 14]. Similarly, using the decay time τ given by the same signal, the viscosity η can be determined [15] by

$$\eta = \frac{\rho r_0^2}{5\tau}. \tag{2}$$

During the experiments, the video images from a high-resolution camera were recorded. After the experiment, each value of the radius at each oscillation was obtained by image analysis. This procedure eliminated the measurement error due to sample evaporation. Moreover, the aspect ratio of the sample (ratio between the horizontal and vertical radii) was also calculated to evaluate the experimental error induced by sample rotation.

While measuring surface tension and viscosity, liquid samples were intentionally rotated to suppress the excitation of oscillation modes other than the $P_2\cos(\theta)$-mode. On the other hand, the characteristic oscillation

frequency ω_c and the decay time τ were dependent on the rotation rate of the liquid sample Ω, by the following equations [16, 17];

$$\frac{\Delta\omega_c}{\omega_c} = \frac{19}{21}\left(\frac{\Omega}{\omega_c}\right)^2 \tag{3}$$

$$\frac{1}{\tau+\Delta\tau} = \frac{1}{\tau}\left[1-\frac{2}{3}\left(\frac{\Omega}{\omega_c}\right)^2\right] \tag{4}$$

where $\Delta\omega_c$ and $\Delta\tau$ are deviations of the characteristic oscillation frequency and decay time due to the rotation, respectively. Unfortunately, rotation rate measurements used for the solid sample were not applicable for the liquid sample because of its shiny surface and sphericity. Instead, the rotation rates of the liquid sample were estimated by monitoring the aspect ratio of the sample. Theoretical predictions of the liquid drop shape of rotating drops have been advanced to a high degree of accuracy by Brown and Scriven [18], and Rhim and Ishikawa [19] have confirmed that the liquid drops which are levitated and rotated in electrostatic levitators followed the predictions. Based on the predictions, relations between the aspect ratios of rotating liquid drops and both rotation rates and oscillation frequency can be expressed by

$$\frac{R_{\text{horizontal}}}{R_{\text{vertical}}} \approx 1 + 1.476\times10^{-2}\left(\frac{\Omega}{\omega_c}\right) + 1.2532\left(\frac{\Omega}{\omega_c}\right)^2 - 1.7877\left(\frac{\Omega}{\omega_c}\right)^3 + 3.7385\left(\frac{\Omega}{\omega_c}\right)^4. \tag{5}$$

Using Eqs. (3) to (5), relations between the aspect ratio and $\Delta\omega_c$ or $\Delta\tau$ can be estimated as shown in Fig. 3.

As shown by the dashed line in Fig. 3, if the aspect ratio of a rotating sample is less than 1.02, the reduced sample rotation rate (Ω/ω_c) is less than 0.13 and effects of the sample rotation to both the characteristic oscillation frequency and the decay time should be no greater than 1.5%. In our experiment, the aspect ratio of the levitated sample was always monitored and did not exceed 1.02. Moreover, if the aspect ratios obtained by the image analysis were greater than 1.02, the oscillation data were discarded.

2.3. Experimental Uncertainties

The experimental uncertainty for density measurements is derived from the respective uncertainty measurements for the mass and volume of

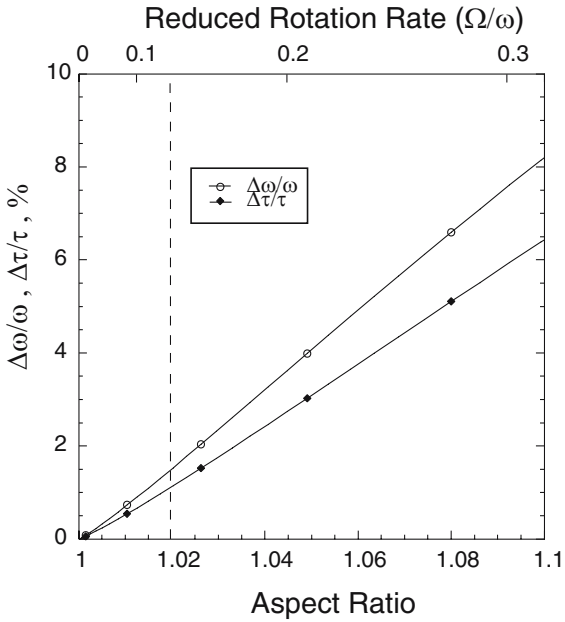

Fig. 3. Relations between the aspect ratio of a rotating liquid drop and the characteristic oscillation frequency, and the decay time.

the samples. Because the uncertainty in the mass is 0.1 mg while a typical iridium sample mass is 50 mg, the uncertainty can be estimated to be approximately 0.2%. As described in Ref. 9, the uncertainty in the volume $(\Delta V/V)$ can be calculated by

$$\frac{\Delta V}{V} = \frac{3\Delta r_0}{r_0} \tag{6}$$

where Δr_0 is the uncertainty in the radius measurement by image analysis. In our experiment, the average value of Δr_0 is around 1 pixel, while r_0 is 160 pixels. Therefore, $\Delta V/V$ can be estimated to be approximately 1.9%, and the overall uncertainty in the density measurement $(\Delta\rho/\rho)$ is estimated to be about 2%.

According to Eq. (1), the uncertainty in the surface tension measurement is mainly determined by those in ρ, r_0, and ω_c. As described earlier, the uncertainty in ρ and r_0 are 2% and 0.65%, respectively. The uncertainty in ω_c induced by the FFT analysis is negligibly small (0.4%) by considering the transformation error (less than 1 Hz) and the typical characteristic oscillation frequency (around 240 Hz). On the other hand, the

1.5% uncertainty on ω_c is induced by the sample rotation, as described in Section 2.2. As a result, the uncertainty in surface tension measurements ($\Delta\gamma/\gamma$) can be estimated to be approximately 3.2% by the following equation:

$$\frac{\Delta\gamma}{\gamma} \approx \sqrt{\left(\frac{\Delta\rho}{\rho}\right)^2 + \left(\frac{3\Delta r_0}{r_0}\right)^2 + \left(\frac{\Delta\omega_c}{\omega_c}\right)^2}. \tag{7}$$

Similarly, using Eq. (2), the uncertainty in the viscosity measurement can be estimated from the uncertainties in ρ, r_0, and τ. The uncertainty in the decay time $\Delta\tau$ is estimated to be about 10%, which is mainly due to the sample motion with respect to the oscillation detector during drop oscillation. This determines the overall uncertainty in the viscosity.

3. EXPERIMENTAL RESULTS

3.1. Density

The density measurements of liquid iridium, taken over the 2300–3000 K temperature range and extending into the supercooled region by nearly 420 K, are shown in Fig. 4. Several data points in Fig. 4 are shown with 2% experimental error bars. The density, like that of other pure

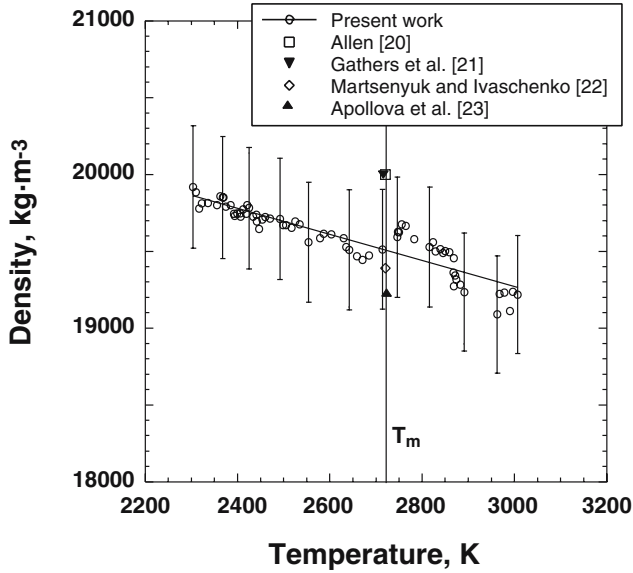

Fig. 4. Density of liquid iridium vs. temperature.

metals, exhibits a linear behavior as a function of temperature and can be fitted by the following relationship with a confidence interval of 95%:

$$\rho(T) = (19.5 \pm 0.2) \times 10^3 - (0.85 \pm 0.09)(T - T_m)(\mathrm{kg \cdot m^{-3}}) \quad (2300 - 3000\,\mathrm{K}) \tag{8}$$

where T_m is the melting temperature (2719 K). To our knowledge, these data were the first to be reported that included such a large temperature excursion into the supercooled region. Around the melting temperature, our value was 2.6% lower than that calculated by Allen [20] and that measured by Gathers et al. [21] with the isobaric expansion method, 0.6% higher than that obtained by Martensyuk and Ivaschenko [22] with the pendent drop method, and 1.4% higher than that measured by Apollova et al. [23] with the sessile drop method.

The volume variation $V(T)$ of the molten state, normalized with the volume at the melting temperature V_m, $(9.9 \times 10^{-6} \mathrm{m^3 \cdot mol^{-1}})$ is derived from Eq. (8), and can be expressed by

$$V(T)/V_m = 1 + 4.4 \times 10^{-5}(T - T_m) \qquad (2300 - 3000\ \mathrm{K}) \tag{9}$$

where 4.4×10^{-5} $(\mathrm{K^{-1}})$ represents the volume expansion coefficient.

The relatively large deviation from the linear fit above the melting temperature was caused by the movement of the sample. Even though the heating lasers were controlled so that horizontal motion of the sample caused by the photon pressure was minimized, a small amount of unbalance remained, and the effect became larger at higher temperatures. Re-design of the electrodes is being conducted to strengthen the horizontal position control to solve this problem.

3.2. Surface Tension

Figure 5 depicts the results for the surface tension of iridium. Several data points in Fig. 5 are accompanied with 3.2% error bars to indicate the experimental uncertainty described in 2.3. Data available from the literature were superimposed on the same figure for comparison. The surface tension data, measured over the 2373–2833 K temperature range and extending into the undercooled region by 346 K, can be expressed with a confidence interval of 95% by

$$\gamma(T) = (2.23 \pm 0.06) \times 10^3 - (0.17 \pm 0.02)(T - T_m)(10^{-3}\mathrm{N \cdot m^{-1}}) \quad (2373 - 2833\ \mathrm{K}). \tag{10}$$

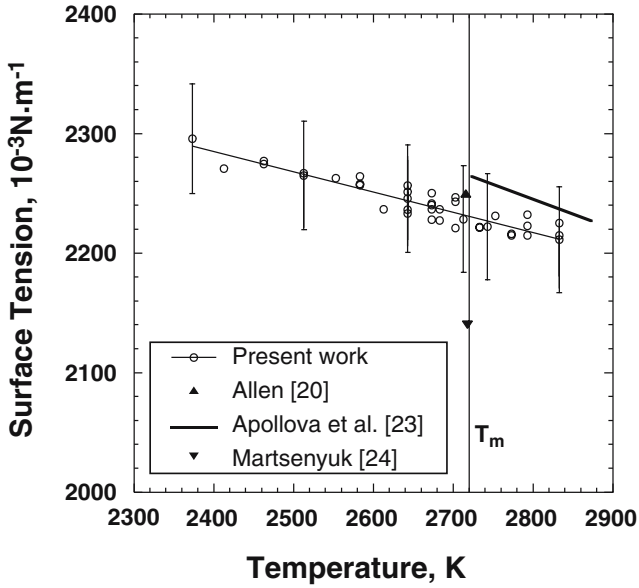

Fig. 5. Surface tension of iridium vs. temperature.

These measurements are the first to cover a large temperature interval over the supercooled as well as equilibrium liquid regions. At the melting temperature, our result was 1% lower than that obtained by Allen [20] and around 2% lower than the value reported by Appollova et al. [23], both of which are within the experimental error. On the other hand, our result was 4.3% higher than that measured by Martsenyuk [24].

3.3. Viscosity

By extracting decay times from the drop oscillation signals, it was possible to determine the viscosities of the liquid iridium over the 2373–2773 K range. Figure 6 illustrates our data with 10 % error bars that can be fitted by the following Arrhenius function:

$$\eta(T) = 1.85 \exp[3.0 \times 10^4/(RT)](10^{-3}\text{Pa}\cdot\text{s}) \qquad (2373 - 2773\ \text{K}), \quad (11)$$

where R, the gas constant, is equal to 8.31 J·mol^{-1}·K^{-1}. The scatter observed in the data is also due to the motion of the sample with respect to the oscillation detector. No other values were found in the literature for comparison.

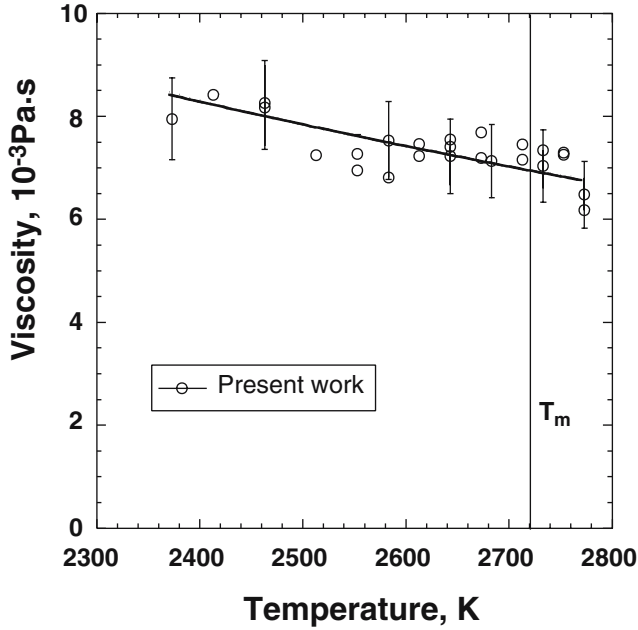

Fig. 6. Viscosity of iridium vs. temperature.

4. CONCLUSIONS

Thermophysical properties of liquid iridium were measured with an electrostatic levitator. For the first time, the viscosity of liquid iridium was reported. Also given in this paper were the density, the thermal expansion coefficient, and the surface tension over wide temperature ranges covering both the supercooled liquid and equilibrium liquid states.

ACKNOWLEDGMENT

We would like to express our deepest gratitude to the Japan Society for the Promotion of Science for their Grant-in-Aid for Scientific Research (B).

REFERENCES

1. D. R. Lide and H. P. R. Frederikse, eds., *CRC Handbook of Chemistry and Physics*, 78th Ed. (CRC Press, Boca Raton, Florida, 1997).

2. Y. Yamabe-Mitarai, Y. Ro, T. Maruko, and H. Harada, *Met. Mat. Trans. A* **29A**:537 (1998).
3. P.-F. Paradis, T. Ishikawa, and S. Yoda, *ESA SP-454*, 993 (2001).
4. T. Ishikawa, P. -F. Paradis, and S. Yoda, *J. Jpn. Soc. Microg. Appl.* **18**:106 (2001).
5. W.-K. Rhim, S.-K. Chung, D. Barber, K.-F. Man, G. Gutt, A. A. Rulison, and R. E. Spjut, *Rev. Sci. Instrum.* **64**:2961 (1993).
6. W.-K. Rhim and T. Ishikawa, *Rev. Sci. Instrum.* **69**:3628 (1998).
7. W.-K. Rhim and P. -F. Paradis, *Rev. Sci. Instrum.* **70**:4652 (1999).
8. T. Ishikawa, P.-F. Paradis, and S. Yoda, *Rev. Sci. Instrum.* **72**:2490 (2001).
9. S.-K. Chung, D. B. Thiessen, and W.-K. Rhim, *Rev. Sci. Instrum.* **67**:3175 (1996).
10. R. W. Hyers, D. M. Matson, K. F. Kelton, and J. R. Rogers, *Proc. Microgravity Transport Processes in Fluid, Thermal, Biological and Materials Sciences III*, Davos, Switzerland (2003).
11. L. Rayleigh, *Proc. R. Soc. London* **29**:71 (1879).
12. W.-K. Rhim, K. Ohsaka, and P.-F. Paradis, *Rev. Sci. Instrum.* **70**:2996 (1999).
13. L. Rayleigh, *Philos. Mag.* **14**:184 (1882).
14. J. Q. Feng and K. V. Beard, *Proc. R. Soc. London* **A 430**:133 (1990).
15. H. Lamb, *Hydrodynamics,* 6th Ed. (Cambridge University Press, 1932), p. 473.
16. F. H. Busse, *J. Fluid Mech.* **142**:1 (1984).
17. C. P. Lee, M. J. Lyell, and T. G. Wang, *Phys. Fluids* **28**:3187 (1985).
18. R. A. Brown and L. E. Scriven, *Proc. R. Soc. London* **A 371**: 331 (1980).
19. W.-K. Rhim and T. Ishikawa, *Rev. Sci. Instrum.* **72**:3572 (2001).
20. B. C. Allen, *Trans. AIME* **227**:1175 (1963).
21. G. R. Gathers, J. W. Shaner, R. S. Hixson, and D. A. Jung, *High Temp.-High Press.* **11**:653 (1979).
22. P. S. Martsenyuk and Yu. V. Ivaschenko, *Ukr. Khim. Zhur. (SU)* **40**:431 (1974).
23. T. A. Apollova, E. L. Dubinin, M. M. Mitko, A. I. Chegodayev, and L .L. Bezuladnkova, *Izv. Akad. Nauk SSSR, Met.***6**:55 (1982).
24. P. S. Martsenyuk, *Inst. Tekh. Probl. Mater. Akad. Nauk SSSR* 51–57 (1980).